Report

Current Biology

An Exceptionally Preserved Three-Dimensional Armored Dinosaur Reveals Insights into Coloration and Cretaceous Predator-Prey Dynamics

Graphical Abstract

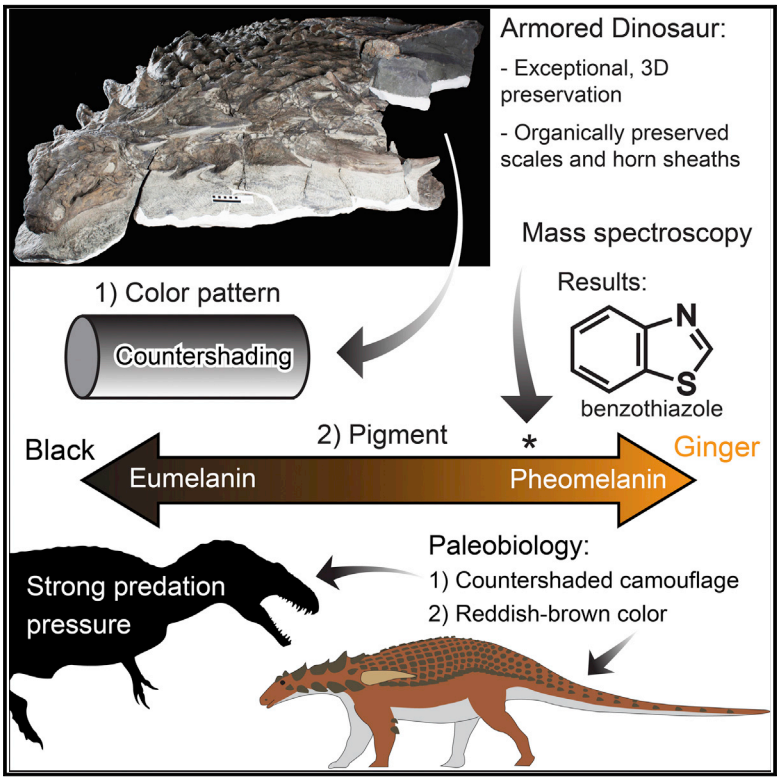

Highlights

- A new armored dinosaur is described based on an exceptionally preserved specimen
- Abundant *in situ* osteoderms with keratinous sheaths and scales are preserved
- Reddish-brown coloration and crypsis in the form of countershading are indicated
- Crypsis indicates strong predation pressure on this large, heavily armored dinosaur

Authors

Caleb M. Brown, Donald M. Henderson, Jakob Vinther, Ian Fletcher, Ainara Sistiaga, Jorsua Herrera, Roger E. Summons

Correspondence

caleb.brown@gov.ab.ca

In Brief

Brown et al. report a new, exceptionally preserved armored dinosaur, showing bony armor with horn coverings and organically preserved scales. A reddish-brown coloration and camouflage in the form of countershading are indicated. Crypsis suggests strong visual predation pressure on this heavily armored dinosaur, distinct from modern systems.

Brown et al., 2017, Current Biology *27*, 1–8
August 21, 2017
http://dx.doi.org/10.1016/j.cub.2017.06.071

CellPress

Please cite this article in press as: Brown et al., An Exceptionally Preserved Three-Dimensional Armored Dinosaur Reveals Insights into Coloration and Cretaceous Predator-Prey Dynamics, Current Biology (2017), http://dx.doi.org/10.1016/j.cub.2017.06.071

Current Biology
Report

An Exceptionally Preserved Three-Dimensional Armored Dinosaur Reveals Insights into Coloration and Cretaceous Predator-Prey Dynamics

Caleb M. Brown,[1,6,*] Donald M. Henderson,[1] Jakob Vinther,[2,3] Ian Fletcher,[4] Ainara Sistiaga,[5] Jorsua Herrera,[5] and Roger E. Summons[5]
[1]Royal Tyrrell Museum of Palaeontology, PO Box 7500, Drumheller, AB T0J 0Y0, Canada
[2]School of Biological Sciences, University of Bristol, Life Sciences Building, 24 Tyndall Avenue, Bristol BS8 1TQ, UK
[3]School of Earth Sciences, University of Bristol, Wills Memorial Building, Queens Road, Bristol BS8 1RJ, UK
[4]School of Mechanical and Systems Engineering, Newcastle University, Newcastle NE1 7RU, UK
[5]Department of Earth, Atmospheric and Planetary Sciences, Massachusetts Institute of Technology, 45 Carleton St., Cambridge, MA 02142, USA
[6]Lead Contact
*Correspondence: caleb.brown@gov.ab.ca
http://dx.doi.org/10.1016/j.cub.2017.06.071

SUMMARY

Predator-prey dynamics are an important evolutionary driver of escalating predation mode and efficiency, and commensurate responses of prey [1–3]. Among these strategies, camouflage is important for visual concealment, with countershading the most universally observed [4–6]. Extant terrestrial herbivores free of significant predation pressure, due to large size or isolation, do not exhibit countershading. Modern predator-prey dynamics may not be directly applicable to those of the Mesozoic due to the dominance of very large, visually oriented theropod dinosaurs [7]. Despite thyreophoran dinosaurs' possessing extensive dermal armor, some of the most extreme examples of anti-predator structures [8, 9], little direct evidence of predation on these and other dinosaur megaherbivores has been documented. Here we describe a new, exquisitely three-dimensionally preserved nodosaurid ankylosaur, *Borealopelta markmitchelli* gen. et sp. nov., from the Early Cretaceous of Alberta, which preserves integumentary structures as organic layers, including continuous fields of epidermal scales and intact horn sheaths capping the body armor. We identify melanin in the organic residues through mass spectroscopic analyses and observe lighter pigmentation of the large parascapular spines, consistent with display, and a pattern of countershading across the body. With an estimated body mass exceeding 1,300 kg, *B. markmitchelli* was much larger than modern terrestrial mammals that either are countershaded or experience significant predation pressure as adults. Presence of countershading suggests predation pressure strong enough to select for concealment in this megaherbivore despite possession of massive dorsal and lateral armor, illustrating a significant dichotomy between Mesozoic predator-prey dynamics and those of modern terrestrial systems.

RESULTS AND DISCUSSION

Systematic Paleontology

Dinosauria Owen, 1842 [10].
Ornithischia Seeley, 1888 [11].
Ankylosauria Osborn, 1923 [12].
Nodosauridae Marsh, 1890 [13].
Borealopelta markmitchelli gen. et sp. nov. (Figures 1 and 2).

Etymology

The generic name *Borealopelta* is derived from "borealis" (Latin, "northern") and "pelta" (Greek, "shield"), in reference to the northern locality and the preserved epidermal scales and dermal osteoderms. The specific epithet *markmitchelli* honors Mark Mitchell for his more than 7,000 hours of patient and skilled preparation of the holotype.

Holotype

The holotype is Royal Tyrrell Museum of Palaeontology (TMP) 2011.033.0001: an articulated specimen preserving the head, neck, most of the trunk and sacrum, a complete right and a partial left forelimb and manus, partial pes (Figure 1). *In situ* osteoderms and nearly complete soft tissue integument are preserved across dorsal and lateral surfaces of the axial skeleton, posterodorsal surface of forelimbs, and plantar surfaces of a manus and a pes. Specimen is preserved in multiple large blocks, including slabs and counter-slabs in the sacral region.

Locality and Horizon

Suncor Millennium Mine, Fort McMurray, Alberta, Canada. Wabiskaw Member, Clearwater Formation, Aptian stage. Detailed locality data are available at Royal Tyrrell Museum of Palaeontology.

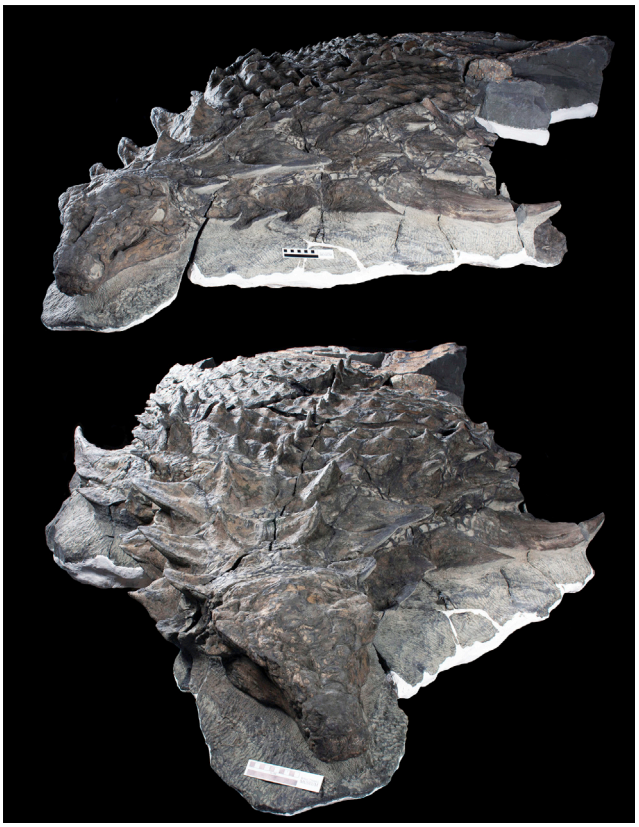

Figure 1. Photographs of the Holotype of *Borealopelta markmitchelli*, TMP 2011.033.0001

Top: anterodorsolateral view; bottom: anterodorsal view. Scale bar, 10 cm. See also Figure S1.

Diagnosis

A nodosaurid ankylosaur characterized by the following autapomorphies (*) and suite of characters [character/state]: cranial: dorsal skull ornamentation expressed as a large hexagonal dermal plate in frontoparietal region [52:1] and multiple (>20) small dermal plates in frontonasal region [21:2]*; external nares excluded from view dorsally (shared with *Pawpawsaurus*) [16:1]; supraorbital ornamentation forming sharp lateral rim dorsal to orbits (shared with *Gargoyleosaurus* and *Kunbarrasaurus*) [38:2]; jugal (suborbital) horn triangular with pointed apex (shared with *Gastonia*, *Gargoyleosaurus*, and *Polocanthus*) [47:2]; jugal (suborbital) horn base longer than orbit length [49:2]*; osteoderms: cervical and thoracic osteoderms form continuous (abutting) transverse rows completely separated by continuous transverse rows of polygonal basement scales; parascapular spine is the largest osteoderm, recurved, and projects posterolaterally and horizontally (potentially shared with *Sauropelta*); osteoderm count for transverse rows: cervicals: C1-3, C2-3, C3-3, transition: TR-2, thoracic: T1-6*; third and sixth transverse thoracic osteoderm rows expressed medially but pinch out laterally*.

The new taxon can be further differentiated from *Pawpawsaurus* based on: dermal plate in frontonasal region (central dermal plates) flat [22:1]; absence of ciliary osteoderm [41:0]. Can be further differentiated from *Sauropelta* based on: parietals flat to slightly convex [51:0]; cervical half ring has 4–6 osteoderms only [164:1]; medial cervical osteoderms subequal, hexagonal, and bear prominent median ridge with posterior margin projecting beyond the basal footprint.

Morphological Description

For a morphological description of the head, osteoderms, epiosteodermal scales (osteoderm/spine horn sheaths), and epidermal basement scales, see the Supplemental Morphological Description.

Phylogenetic Analysis

To determine the phylogenetic position of *Borealopelta markmitchelli*, we scored it into the morphological character/taxon matrix of Arbour et al. [14] (see also STAR Methods for full phylogenetic methods, Data S1 for data, and Supplemental Phylogenetic Results). The resulting strict consensus tree positions *Borealopelta* in a clade with other Albian-aged nodosaurids *Pawpawsaurus campbelli* and *Europelta carbonensis*, with the Santonian-aged *Hungarosaurus tormai* as a sister taxon (Figures 3 and S2).

Deposition and Preservation History

The specimen was discovered in the Suncor Millennium Mine (open pit, oil sands) in northeastern Alberta, Canada during overburden removal and was subsequently collected by staff of the Royal Tyrrell Museum and Suncor. The hosting rock is the Albian-aged Wabiskaw Member of the Clearwater Formation overlying the bitumen-rich McMurray Formation. Several plesiosaurs and ichthyosaurs have been recovered from the Wabiskaw previously [15–17], but never a dinosaur. This member records a lower shoreface or proximal offshore marine environment [15]. The carcass arrived at the seabed on its back and with sufficient force to impact and deform the immediately underlying sedimentary layers. Despite the trace fossils left by burrowing animals in the hosting sediments, implying at least a partially oxygenated environment, the specimen lacks any evidence of scavenging. When found, the fossil was completely encased in a very dense and strong but brittle siderite concretion that ranged in thickness around the carcass from 20 cm on the upper side to 40 cm on the lower, seabed side. Broken surfaces through the concretion reveal sedimentary features above the fossil that allow for inferring the natural collapse of the body after burial and before consolidation (Figure S4i). About 15 cm of sediment was laid down prior to release of internal body fluids and collapse (Figure S4i), evidenced from a collapse/fluid escape structure in the sacral region (Figure S4i). The body cavity was injected with almost homogeneous sand, with no apparent sedimentary features. Formation of the concretion must have commenced shortly after the carcass arrived at the seabed, preventing any scavenging and allowing all of the scales and osteoderms to retain their original configurations and morphology, with minimal dorsoventral compression.

The dorsal integument is well preserved as an organic film derived from the keratin sheaths over the osteoderms, integumentary scales, and the epicuticle of hinge regions between scales. The distribution of the film correlates well to the expected distribution of melanin, a pigment that has been found to preserve in a number of vertebrate integumentary structures

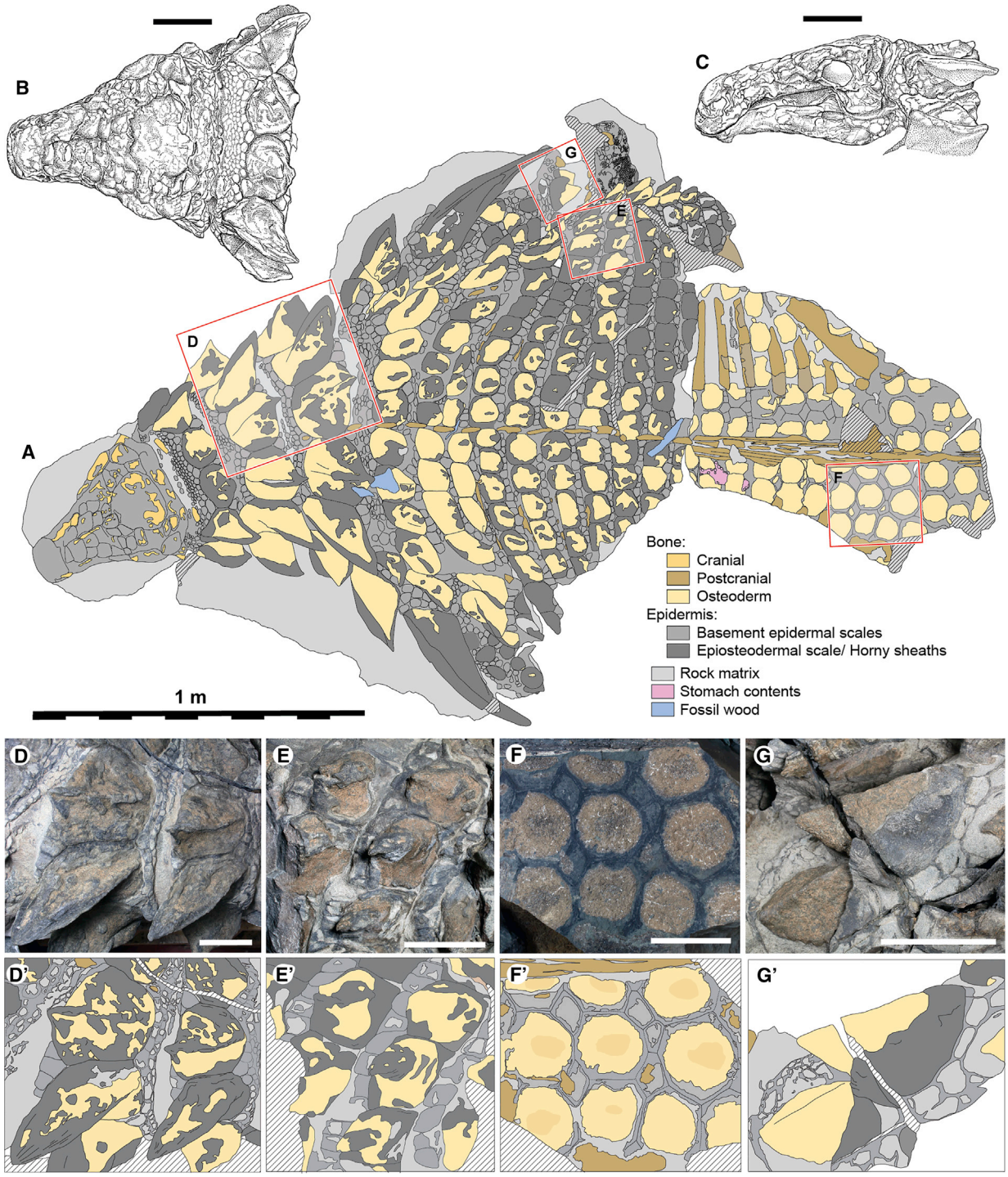

Figure 2. Schematic Line Drawing of TMP 2011.033.0001, the Holotype of *Borealopelta markmitchelli*, Illustrating Preservation of the Different Tissue Types

(A) Schematic of complete specimen in dorsal view.

(B and C) Skull in dorsal (B) and left lateral (C) views.

(D) Close-up view of the neck, illustrating alternating cervical osteoderm bands (and preserved keratinous sheaths) and polygonal scales.

(E) Close-up view of flank illustrating lateral thoracic osteoderms (with keratinous coverings) and polygonal scales.

(F) Close-up view of sacral shield counterpart illustrating osteoderms and scales.

(G) Close-up view of antebrachium including osteoderms and keratinous coverings.

(D'–G') Interpretive line drawings of the corresponding panels (D)–(G).

Scale bars in (B)–(G), 10 cm. See also Figure S1.

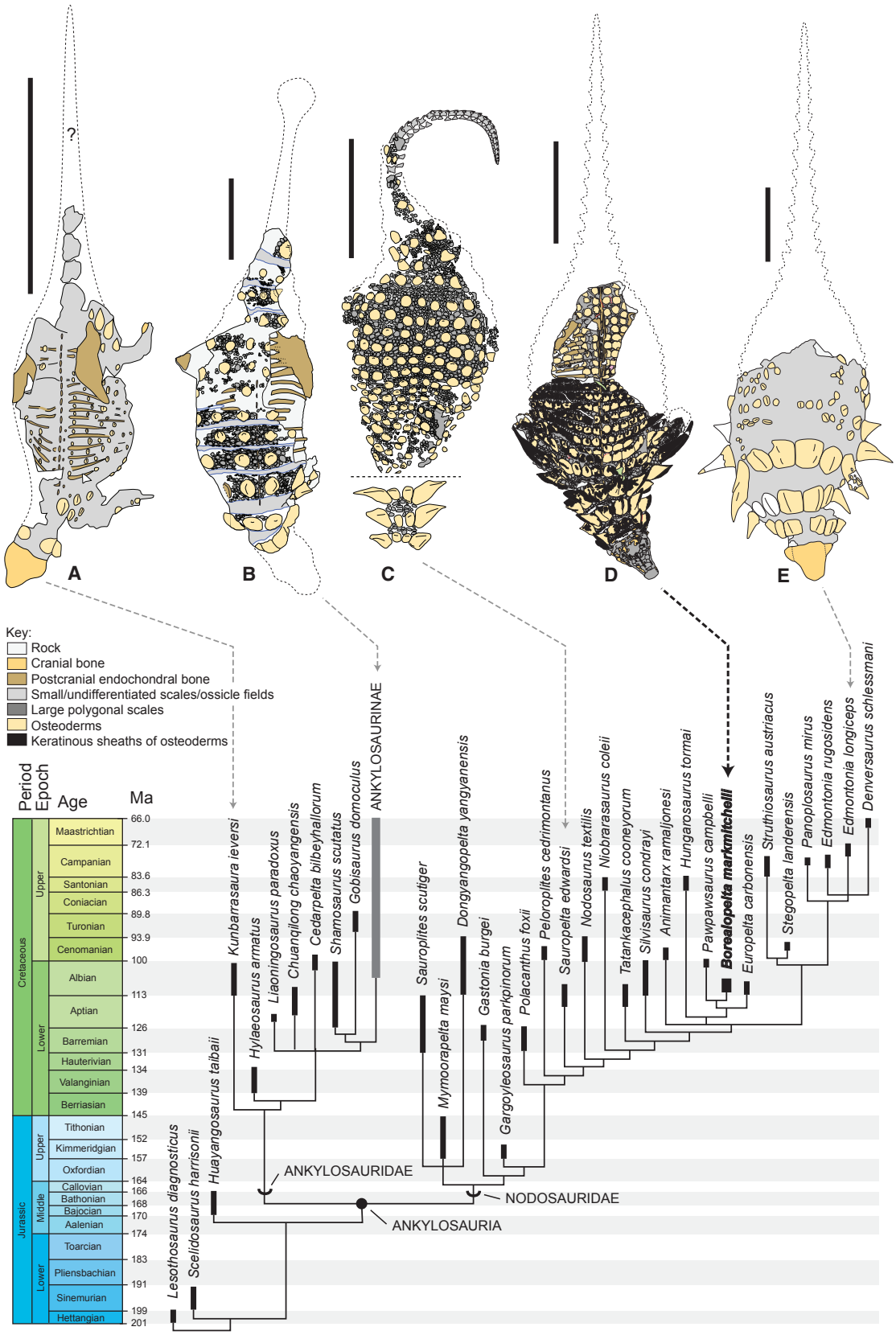

(legend on next page)

[6, 18, 19]. Scanning electron microscopy (SEM) and energy-dispersive X-ray spectroscopy (EDAX) analyses reveal that the organic material is present as solid to finely granular material with desiccation cracks scattered in a matrix largely composed of siderite cement (Figure S3ii; see also STAR Methods and Supplemental Observations Under the Electron Microscope). No apparent melanosomes are preserved. Time-of-flight secondary ion mass spectrometry (TOF-SIMS) reveals spectra of negative secondary ions that have an overall relative secondary ion intensity similar to previously studies of fossil melanins (Figure S3iiiA; see also STAR Methods and Supplemental Results from the TOF SIMS). Principal-component analyses demonstrate that there is a significant contribution of sulfur-bearing secondary ions to the organic material in TMP 2011.033.0001, which spread the nodosaur samples distinctly from other fossil melanin samples (Figure S3iiiB). These secondary ions have been identified for sulfur-bearing pheomelanin (benzothiazole) previously [19]. Pyrolysis-gas chromatography-mass spectroscopy (py-GC-MS) afforded pyrolysates with assemblages of small nitrogen-, oxygen- and sulfur-containing heterocyclic and aromatic molecules characteristic of eumelanin (e.g., pyrrole, indole, N-methylpyrrole, and methylphenol). Of special note is the presence of significant amounts of benzothiazole (Figure S3iv), which is diagnostic for pheomelanin. Although sulfur may be incorporated into melanin secondarily [20] to yield thiophenes, which are also observed and could similarly be derived from pheomelanin, this process is not known to give rise to benzothiazoles [20] (see also STAR Methods and Supplemental Results of Pyrolysis GC-MS).

Hence, we argue that the integument was pigmented reddish-brown by pheomelanin-rich melanin. This may also explain the lack of melanosome preservation, as pheomelanin-rich melanosomes have been shown to be less stable in heat/pressure autoclave experiments [18], as well as in enzymatic extraction procedures [21].

Pigment Distribution

Hardened keratinous tissues such as claws, scales, and feathers have reinforcing calcium phosphate deposits [22], which often preserve well in fossil tissues and can be identified using fluorescence imaging [6, 23]. However, the keratinized tissues in TMP 2011.033.0001 are heavily pigmented, which masks calcium phosphate fluorescence [6]. These keratinous sheaths are inert (non-fluorescing and non-reflecting) under UV light, with two major exceptions.

Several cervical osteoderm sheaths show underlying longitudinal ridges that appear to have been unpigmented, as they are dramatically lighter in visible light and exhibit strong fluorescence in UV (Figures S4iiiA–D). These unpigmented longitudinal striae lie in the same plane as the inferred direction of growth of the sheath (i.e., parallel to the *stratum germinativum*) and may represent some preserved artifact of appositional growth of these epiosteodermal scales, as seen in living crocodilians [24, 25].

The largest of the horn sheaths, the parascapular spines, are distinct from the remaining sheaths and epiosteodermal scales in being both lighter colored in visible light and slightly fluorescing under UV light (Figures S4iiiE–H). This is most simply interpreted as having lower concentrations of melanin incorporated into the horn sheath and likely reflects a distinct lighter color of these spines in life.

The contrast in fossilization between the ventral and dorsal surface provides a further case for melanin preservation, as this transition is best interpreted as countershading. Other epidermal structural molecules such as keratin [26, 27] or collagen [28] would have had a very similar distribution in the epidermis on both top and bottom surfaces, and no unique protein markers (amides, succinimides, diketopiperazines) were recovered in the py-GC-MS data to the exclusion of markers overlapping with melanins [29] (Figure S3iv).

The countershading transition can be traced from cross-sectional views of the sacrum (Figure S4ii) and neck. The organic film terminates a little beyond the ventralmost lateral osteoderms. Projecting the melanin distribution to a retrodeformed body outline suggests a transition from highly pigmented to less pigmented integument on the lateral flank (Figure S4ii; see also Supplemental Discussion on the Chemical Preservation of Melanin).

Implications for Paleobiology

The discovery of a three-dimensionally preserved ankylosaurian provides new evidence for understanding the anatomy, soft tissue outline, and arrangement of dermal armor in thyreophoran dinosaurs.

The preservation of the nearly complete integument, along with a suite of *in situ* pre-caudal osteoderms and their horn sheaths, allows multiple novel inferences regarding the epidermis of the ancient animal. Across all preserved regions, the epidermal covering (“epiosteodermal scales” *sensu* [30]) associated with the osteoderms is highly congruous in having a 1:1 correlation in count and basal shape between epidermal scale and underlying osteoderm. This epidermal scale/osteoderm association is most analogous, and potentially deeply homologous, to that observed in extant crocodilians [31, 32].

The epidermal coverings for the thoracic and sacral osteoderms are best interpreted as single, sub-centimeter-thick, keratinized scales (scutes) that slightly exaggerate the keels and spines. In contrast, the epidermal components of the spine-like cervical, transitional, and parascapular osteoderms are

Figure 3. Time-Calibrated Strict Consensus Tree Showing Position of *Borealopelta markmitchelli* within Ankylosauria, with Representative Well-Preserved Ankylosaurs Shown Above

Bottom: time-calibrated strict consensus tree illustrating position of *Borealopelta markmitchelli* within Ankylosauria scaled to Jurassic and Cretaceous stages. Top: line drawings of representative well-preserved ankylosaur specimens with *in situ* armor and/or skin. Scale bars, 1 m. See also Figure S2 and Data S1.

(A) *Kunbarrasaurus*, QM F18101.

(B) *Euoplocephalus*, NHMUK 5161.

(C) *Sauropelta*, AMNH 3035 and 3036 composite.

(D) *Borealopelta*, TMP 2011.033.0001 (this study).

(E) *Edmontonia*, AMNH 5665.

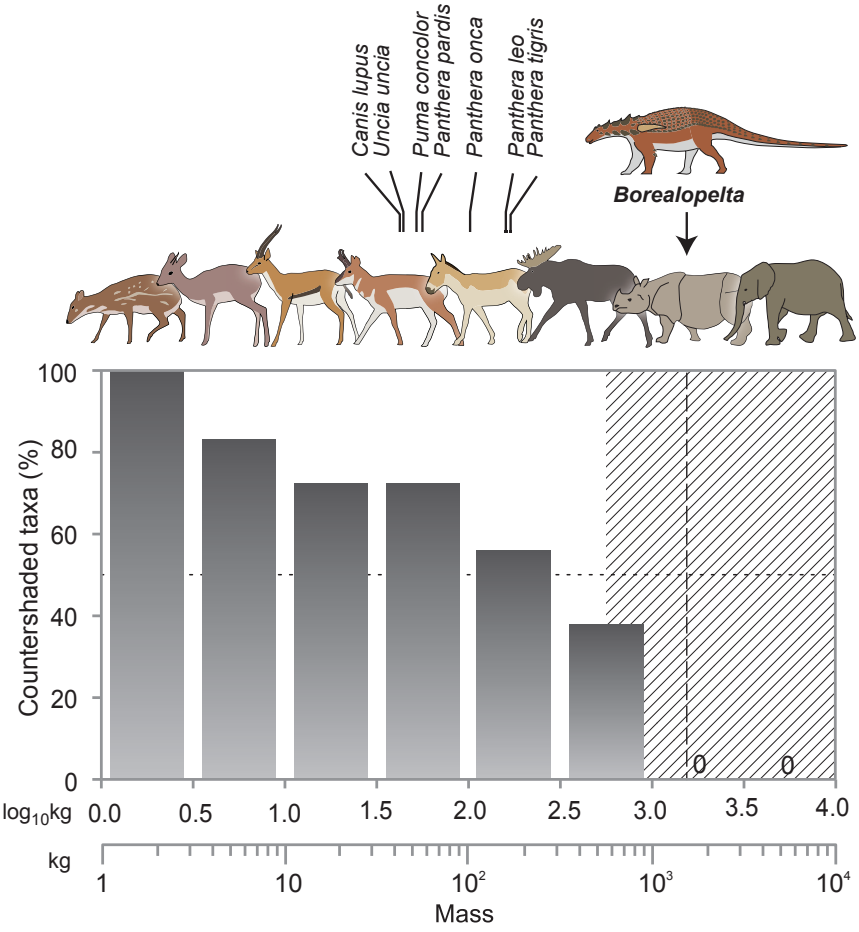

Figure 4. Chart Illustrating the Loss of Countershading as Body Mass Increases in Terrestrial Mammal Herbivores

Chart includes pooled data for artiodactyls, perissodactyls, and proboscideans divided into body-mass bins, showing relative proportion of species that exhibit countershading. The diagonally hatched area represents the mass above which significant predation of adults does not occur. Animals illustrated above chart are representative taxa within each mass bin; species names in italics at top indicate body masses of the largest carnivores. See also Data S2.

sheath-like, being thick, pointed, and extending significantly beyond the bony core, substantially increasing the length of the spine. The macroscopic structure and incorporation of hardening calcium phosphate into the spine-like epiosteodermal scales is broadly similar to the keratinized horn sheaths in Bovidae.

Historically, the function of osteoderms within Ankylosauria has largely been discussed within the context of anti-predator defense, with the term "armor" used ubiquitously to describe these dermal components of the skeleton [9, 33]. More recently, other potential functions including thermoregulation [34–36] and intraspecific combat and display [37] have been proposed, often to augment the seemingly default function as defensive armor. Preserved evidence of countershading suggests that the predation pressure on *Borealopelta*, even at large adult size, was strong enough to select for camouflage from visual predators (see also Supplemental Discussion of Countershading and Body Mass and Data S2). This offers support to the idea that many of the osteoderms functioned in a defensive role, even in adults of large species. In contrast, the distinct pigmentation and enlarged keratinous sheath of the parascapular spine suggest that this particular spine may have functioned more predominantly in display. When combined with data indicating highly species-specific morphology of the parascapular spines of other taxa, this suggests that the extensive elaboration of these spines may be attributable to sociosexual display.

The presence of countershading in a large, heavily armored herbivorous dinosaur provides a unique insight into the predator-prey dynamic of the Cretaceous Period. With an estimated length of 5.5 m and a conservative body mass estimate of ~1,300 kg (similar to estimates for other nodosaurids, i.e., *Sauropelta* [38], but also see higher estimates [39, 40]), *Borealopelta* is much larger than any modern terrestrial animal exhibiting countershading. Modern mammalian predators do not represent a significant predatory risk to the largest mammalian herbivores (>1,000 kg) [41, 42], and herbivores above this size threshold generally do not exhibit countershading or other types of camouflage (Figure 4). Additionally, herbivores below this threshold that also possess defensive weapons (e.g., horn, quills) experience lower predation than those that do not [42]. Similarly, large primates are less likely to be countershaded due to lower predation risk [43]. A parallel pattern is also seen in Testudinidae, where island forms, which are free of significant adult predation, consistently become large [44, 45] and lose the cryptic pattern seen in smaller relatives.

The terrestrial predator guild for most of the Mesozoic was dominated by large non-avian theropod dinosaurs [46]. Although the present specimen is not preserved in the context of its accompanying fauna, the consistent occurrence of large theropod footprints (e.g., *Irenesauripis*) in coeval and nearby formations in northern Alberta and British Columbia [47, 48], and allosauroid/carcharodontosaurid taxa (i.e., *Acrocanthosaurus*) in equivalent formations farther south [49, 50], suggests that the ecosystem of which *Borealopelta* was a part would have included one or more large, multi-ton predatory theropods. Given modern birds' possession of tri- and tetrachromatic vision [51, 52] and the visual acuity of extant crocodilians [53], theropod carnivores would have been highly visual predators [54, 55]. This is in contrast to modern systems in which top predators of large herbivores are dichromatic mammalian carnivores [56]. Active predation on large and heavily armored herbivorous dinosaurs highlights how distinct the predator-prey dynamics of the Cretaceous were from those of today. The greater size and deep visual reliance of

Cretaceous apex predators, compared to extant mammalian analogs, may have produced an evolutionary arms race resulting in a combination of armor, crypsis, and other visual defense strategies in even the largest dinosaurs.

STAR★METHODS

Detailed methods are provided in the online version of this paper and include the following:

- KEY RESOURCES TABLE
- CONTACT FOR REAGENT AND RESOURCE SHARING
- EXPERIMENTAL MODELS AND SUBJECTS
- METHOD DETAILS
  - Computer Tomography Scanning
  - Sampling for Scanning Electron Microscopy and Geochemical Analysis
  - Scanning Electron Microscopy
  - Time-of-Flight Secondary Ion Mass Spectroscopy
  - Pyrolysis Gas Chromatography-Mass Spectrometry
  - Photography
- QUANTIFICATION AND STATISTICAL ANALYSIS
  - Phylogenetic Methods
- DATA AND SOFTWARE AVAILABILITY
  - Specimen
  - Nomenclature

SUPPLEMENTAL INFORMATION

Supplemental Information includes four figures, supplemental text, and two datasets and can be found with this article online at http://dx.doi.org/10.1016/j.cub.2017.06.071.

AUTHOR CONTRIBUTIONS

D.M.H. was part of the team that excavated the specimen. C.M.B. and D.M.H. performed the description and phylogenic analyses. J.V. performed the SEM and EDAX analyses and planned the strategy for chemical analyses. I.F. and J.V. performed the TOF-SIMS analyses. A.S., J.H., and R.E.S. performed the pyrolysis GC-MS analyses. J.V., C.M.B., and D.M.H. analyzed the ecological implications of coloration in *B. markmitchelli*. All authors contributed to the manuscript.

ACKNOWLEDGMENTS

We thank Shawn Funk for the initial discovery of the specimen and Mike Gratton, Doug Lacey, Bob Herron, Hans Heltke, Steve Hill, Ryan McPhearson, and many tens of Suncor Energy employees for assistance in excavation of the specimen. We recognize the technical skills of Darren Tanke (RTMP) that enabled the collection of the specimen. Jim McCabe (RTMP) delivered key supplies to the worksite. Mark Mitchell committed nearly six years to the preparation of the specimen, and many RTMP preparation, collection, and fabrication staff assisted with the project. Donna Sloan produced scientific illustrations of the specimen (Figures 2B, 2C, and S1). Sue Sabrowski, Corey Jaskolski, and Ann Jaskolski assisted with specimen photography. CT scans were performed at Western Veterinary Specialist and Emergency Centre, Calgary, with the assistance of Nic Roussset, Joni Klaassen, and Cathy Gaviller. Xander Warren assisted with SEM and EDAX analyses. TNT software was made available through the Willi Hennig Society. We also thank Don Brinkman, Michael Burns, David Eberth, Aurora Elmore, Michael Habib, Michael Greshko, Carrie-Anne Lunde, Mark Mitchell, Matthew Piscitelli, Patty Ralrick, and Anthony Russell for discussions and assistance. Steve Brusatte, Florian Maderspacher (the scientific editor), and an anonymous reviewer provided comments that improved the paper. Funding was provided by Suncor Energy, the Royal Tyrrell Museum of Palaeontology, the Royal Tyrrell Museum Cooperating Society, the National Geographic Society (10004-16), and the NASA Astrobiology Institute (NNA13AA90A).

Received: March 6, 2017
Revised: May 16, 2017
Accepted: June 27, 2017
Published: August 3, 2017

REFERENCES

1. Vermeij, G.J. (1977). The Mesozoic marine revolution: evidence from snails, predators and grazers. Paleobiology *3*, 245–258.
2. Vermeij, G.J. (1993). Evolution and Escalation: An Ecological History of Life (Princeton University Press).
3. Vermeij, G.J. (1994). The evolutionary interaction among species: selection, escalation, and coevolution. Annu. Rev. Ecol. Syst. *25*, 219–236.
4. Allen, W.L., Baddeley, R., Cuthill, I.C., and Scott-Samuel, N.E. (2012). A quantitative test of the predicted relationship between countershading and lighting environment. Am. Nat. *180*, 762–776.
5. Penacchio, O., Lovell, P.G., Cuthill, I.C., Ruxton, G.D., and Harris, J.M. (2015). Three-dimensional camouflage: exploiting photons to conceal form. Am. Nat. *186*, 553–563.
6. Vinther, J., Nicholls, R., Lautenschlager, S., Pittman, M., Kaye, T.G., Rayfield, E., Mayr, G., and Cuthill, I.C. (2016). 3D camouflage in an ornithischian dinosaur. Curr. Biol. *26*, 2456–2462.
7. Holtz, T.R. (2003). Dinosaur Predation. In Predator-Prey Interactions in the Fossil Record, P.H. Kelley, M. Kowalewski, and T.A. Hansen, eds. (Springer), pp. 325–340.
8. Alexander, R.M. (1997). Engineering a dinosaur. In The Complete Dinosaur, J.A. Farlow, and M.K. Brett-Surman, eds. (Indiana University Press), pp. 414–425.
9. Matthews, W. (1922). A super-dreadnaught of the animal world: The armored dinosaur *Palaeoscincus*. Nat. Hist. *22*, 333–342.
10. Owen, R. (1842). Report on British fossil reptiles, part II. Rep. Br. Assoc. Adv. Sci. *1841*, 60–204.
11. Seeley, H.G. (1888). The classification of the Dinosauria. Rep. Br. Assoc. Adv. Sci. *1887*, 698–699.
12. Osborn, H.F. (1923). Two Lower Cretaceous dinosaurs of Mongolia. Am. Mus. Novit. *95*, 1–10.
13. Marsh, O.C. (1890). Additional characters of the Ceratopsidae, with notice of new Cretaceous dinosaurs. Am. J. Sci. *39*, 418–429.
14. Arbour, V.M., Zanno, L.E., and Gates, T.A. (2016). Ankylosaurian dinosaur palaeoenvironmental associations were influenced by extirpation, sea-level fluctuation, and geodispersal. Palaeogeogr. Palaeoclimatol. Palaeoecol. *449*, 289–299.
15. Druckenmiller, P.S., and Maxwell, E.E. (2010). A new Lower Cretaceous (lower Albian) ichthyosaur genus from the Clearwater Formation, Alberta, Canada. Can. J. Earth Sci. *47*, 1037–1053.
16. Maxwell, E.E., and Druckenmiller, P.S. (2011). A small ichthyosaur from the Clearwater Formation (Alberta, Canada) and a discussion of the taxonomic utility of the pectoral girdle. Paläontologische Zeitschrift *85*, 457–463.
17. Druckenmiller, P.S., and Russell, A.P. (2009). Earliest North American occurrence of Polycotylidae (Sauropterygia: Plesiosauria) from the Lower Cretaceous (Albian) Clearwater Formation, Alberta, Canada. J. Paleontol. *83*, 981–989.
18. Colleary, C., Dolocan, A., Gardner, J., Singh, S., Wuttke, M., Rabenstein, R., Habersetzer, J., Schaal, S., Feseha, M., Clemens, M., et al. (2015). Chemical, experimental, and morphological evidence for diagenetically altered melanin in exceptionally preserved fossils. Proc. Natl. Acad. Sci. USA *112*, 12592–12597.
19. Lindgren, J., Sjövall, P., Carney, R.M., Uvdal, P., Gren, J.A., Dyke, G., Schultz, B.P., Shawkey, M.D., Barnes, K.R., and Polcyn, M.J. (2014).

Skin pigmentation provides evidence of convergent melanism in extinct marine reptiles. Nature *506*, 484–488.

20. Glass, K., Ito, S., Wilby, P.R., Sota, T., Nakamura, A., Bowers, C.R., Vinther, J., Dutta, S., Summons, R., Briggs, D.E.G., et al. (2012). Direct chemical evidence for eumelanin pigment from the Jurassic period. Proc. Natl. Acad. Sci. USA *109*, 10218–10223.
21. Liu, Y., Hong, L., Wakamatsu, K., Ito, S., Adhyaru, B., Cheng, C.Y., Bowers, C.R., and Simon, J.D. (2005). Comparison of structural and chemical properties of black and red human hair melanosomes. Photochem. Photobiol. *81*, 135–144.
22. Pautard, F.G.E. (1964). Calcification of keratin. In Progress in the Biological Sciences in Relation to Dermatology, *Volume 2*, A. Rook, and R.H. Champion, eds. (Cambridge University Press), pp. 227–239.
23. Mayr, G., Pittman, M., Saitta, E., Kaye, T.G., and Vinther, J. (2016). Structure and homology of *Psittacosaurus* tail bristles. Palaeontology *59*, 793–802.
24. Spearman, R.I.C., and Riley, P.A. (1969). A comparison of the epidermis and pigment cells of the crocodile with those in two lizard species. Zool. J. Linn. Soc. *48*, 453–466.
25. Reese, A.M. (1915). The Alligator and Its Allies (Knickerbocker Press).
26. Pan, Y., Zheng, W., Moyer, A.E., O'Connor, J.K., Wang, M., Zheng, X., Wang, X., Schroeter, E.R., Zhou, Z., and Schweitzer, M.H. (2016). Molecular evidence of keratin and melanosomes in feathers of the Early Cretaceous bird Eoconfuciusornis. Proc. Natl. Acad. Sci. USA *113*, E7900–E7907.
27. Moyer, A.E., Zheng, W., and Schweitzer, M.H. (2016). Keratin durability has implications for the fossil record: results from a 10 year feather degradation experiment. PLoS ONE *11*, e0157699.
28. Lingham-Soliar, T., Feduccia, A., and Wang, X. (2007). A new Chinese specimen indicates that 'protofeathers' in the Early Cretaceous theropod dinosaur *Sinosauropteryx* are degraded collagen fibres. Proc. Biol. Sci. *274*, 1823–1829.
29. Saitta, E.T., Rogers, C., Brooker, R.A., Abbott, G.D., Kumar, S., O'Reilly, S.S., Donohoe, P., Dutta, S., Summons, R.E., and Vinther, J. (2017). Low fossilization potential of keratin protein revealed by experimental taphonomy. Palaeontology *60*, 547–556.
30. Arbour, V.M., Burns, M.E., Bell, P.R., and Currie, P.J. (2014). Epidermal and dermal integumentary structures of ankylosaurian dinosaurs. J. Morphol. *275*, 39–50.
31. Vickaryous, M.K., and Sire, J.-Y. (2009). The integumentary skeleton of tetrapods: origin, evolution, and development. J. Anat. *214*, 441–464.
32. Vickaryous, M.K., and Hall, B.K. (2008). Development of the dermal skeleton in *Alligator mississippiensis* (Archosauria, Crocodylia) with comments on the homology of osteoderms. J. Morphol. *269*, 398–422.
33. Romer, A.S. (1945). Vertebrate Paleontology (University of Chicago Press).
34. Carpenter, K. (1982). Skeletal and dermal armor reconstruction of *Euoplocephalus tutus* (Ornithischia: Ankylosauridae) from the Late Cretaceous Oldman Formation of Alberta. Can. J. Earth Sci. *19*, 689–697.
35. Blows, W.T. (2001). Dermal armour of the polacanthine dinosaurs. In The Armored Dinosaurs, K. Carpenter, ed. (Indiana University Press), pp. 363–385.
36. Hayashi, S., Carpenter, K., Scheyer, T.M., Watabe, M., and Suzuki, D. (2010). Function and Evolution of Ankylosaur Dermal Armor. Acta Palaeontol. Pol. *55*, 213–228.
37. Padian, K., and Horner, J.R. (2011). The evolution of 'bizarre structures' in dinosaurs: biomechanics, sexual selection, social selection or species recognition? J. Zool. *283*, 3–17.
38. Carpenter, K. (1984). Skeletal reconstruction and life restoration of *Sauropelta* (Ankylosauria: Nodosauridae) from the Cretaceous of North America. Can. J. Earth Sci. *21*, 1491–1498.
39. Benson, R.B., Campione, N.E., Carrano, M.T., Mannion, P.D., Sullivan, C., Upchurch, P., and Evans, D.C. (2014). Rates of dinosaur body mass evolution indicate 170 million years of sustained ecological innovation on the avian stem lineage. PLoS Biol. *12*, e1001853.
40. Paul, G. (1997). Dinosaur models: the good, the bad, and using them to estimate the mass of dinosaurs. In Dinofest International: Proceedings of a Symposium Sponsored By Arizona State University, D.L. Wolberg, E. Stump, and G.D. Rosenberg, eds. (Academy of Natural Sciences), pp. 39–45.
41. Owen-Smith, N., and Mills, M.G.L. (2008). Predator-prey size relationships in an African large-mammal food web. J. Anim. Ecol. *77*, 173–183.
42. Hayward, M.W., and Kerley, G.I.H. (2005). Prey preferences of the lion (*Panthera leo*). J. Zool. *267*, 309–322.
43. Kamilar, J.M. (2009). Interspecific variation in primate countershading: effects of activity pattern, body mass, and phylogeny. Int. J. Primatol. *30*, 877.
44. Arnold, E.N. (1979). Indian Ocean giant tortoises: their systematics and island adaptations. Philos. Trans. R. Soc. Lond. B Biol. Sci. *286*, 127–145.
45. Jaffe, A.L., Slater, G.J., and Alfaro, M.E. (2011). The evolution of island gigantism and body size variation in tortoises and turtles. Biol. Lett. *7*, 558–561.
46. Zanno, L.E., and Makovicky, P.J. (2013). Neovenatorid theropods are apex predators in the Late Cretaceous of North America. Nat. Commun. *4*, 2827.
47. McCrea, R.T., and Currie, P.J. (1998). A preliminary report on dinosaur tracksites in the Lower Cretaceous (Albian) Gates Formation near Grande Cache, Alberta. N M Mus. Nat. Hist. Sci. Bull. *14*, 155–162.
48. Currie, P.J. (1989). Dinosaur footprints of Western Canada. In Dinosaur Tracks and Traces, D.D. Gillette, and M.G. Lockley, eds. (Cambridge University Press), pp. 293–300.
49. Eddy, D.R., and Clarke, J.A. (2011). New information on the cranial anatomy of *Acrocanthosaurus atokensis* and its implications for the phylogeny of Allosauroidea (Dinosauria: Theropoda). PLoS ONE *6*, e17932.
50. D'Emic, M.D., Melstrom, K.M., and Eddy, D.R. (2012). Paleobiology and geographic range of the large-bodied Cretaceous theropod dinosaur *Acrocanthosaurus atokensis*. Palaeogeogr. Palaeoclimatol. Palaeoecol. *333-334*, 13–23.
51. Vorobyev, M., Osorio, D., Bennett, A.T.D., Marshall, N.J., and Cuthill, I.C. (1998). Tetrachromacy, oil droplets and bird plumage colours. J. Comp. Physiol. A Neuroethol. Sens. Neural Behav. Physiol. *183*, 621–633.
52. Cuthill, I.C., Partridge, J.C., Bennett, A.T.D., Chrurch, S.C., Hart, N.S., and Hunt, S. (2000). Ultraviolet vision in birds. Adv. Stud. Behav. *29*, 159–214.
53. Sillman, A.J., Ronan, S.J., and Loew, E.R. (1991). Histology and microspectrophotometry of the photoreceptors of a crocodilian, *Alligator mississippiensis*. Proc. R. Soc. Lond. B Biol. Sci. *243*, 93–98.
54. Stevens, K.A. (2006). Binocular vision in theropod dinosaurs. J. Vertebr. Paleontol. *26*, 321–330.
55. Rowe, M.P. (2000). Inferring the retinal anatomy and visual capacities of extinct vertebrates. Palaeontol. Electronica *3*, 1–43.
56. Jacobs, G.H. (1993). The distribution and nature of colour vision among the mammals. Biol. Rev. Camb. Philos. Soc. *68*, 413–471.
57. O'Gorman, E.J., and Hone, D.W.E. (2013). Body size distribution of the dinosaurs. PLoS ONE *7*, e51925.
58. Stoner, C.J., Caro, T.M., and Graham, C.M. (2003). Ecological and behavioral correlates of coloration in artiodactyls: systematic analyses of conventional hypotheses. Behav. Ecol. *14*, 823–840.
59. Schwieters, J., Cramer, H.G., Heller, T., Jürgens, U., Niehuis, E., Zehnpfenning, J., and Benninghoven, A. (1991). High mass resolution surface imaging with a time-of-flight secondary ion mass spectroscopy scanning microprobe. J. Vac. Sci. Technol. A *9*, 2864–2871.
60. Crabb, P. (2001). The use of polarised light in photography of macrofossils. Palaeontology *44*, 659–664.
61. Goloboff, P.A., Farris, J.S., and Nixon, K. (2008). TNT, a free program for phylogenetic analysis. Cladistics *24*, 774–786.

STAR★METHODS

KEY RESOURCES TABLE

REAGENT or RESOURCE	SOURCE	IDENTIFIER
Biological Samples		
Borealopelta markmitchelli holotype specimen	This paper	TMP 2011.033.0001
Deposited Data		
Character/taxon matrix for cladistic analysis	This paper (modified from [14])	Data S1
Mammal body mass/coloration data	compiled from [57] and [58]	Data S2
Software and Algorithms		
TNT software	Willi Hennig Society, https://cladistics.org/tnt/	N/A
R software	https://www.r-project.org/	N/A

CONTACT FOR REAGENT AND RESOURCE SHARING

Further information and requests for resources and reagents should be directed to and will be fulfilled by the Lead Contact, Caleb Brown (caleb.brown@gov.ab.ca).

EXPERIMENTAL MODELS AND SUBJECTS

The experimental subject is the fossilized holotype of the nodosaurid dinosaur *Borealopelta markmitchelli* (TMP 2011.033.0001), curated at the Royal Tyrrell Museum of Palaeontology, Drumheller, Alberta, Canada. The sex and developmental state are unknown, although an adult (or nearly adult age) is inferred.

METHOD DETAILS

Computer Tomography Scanning

The skull was CT scanned in an attempt to reveal its internal structure. CT scans were performed at Western Veterinary Specialist and Emergency Centre in Calgary, Alberta, using a Toshiba Aquilion Scanner. A variety scanning parameters were tested, verifying the voltage and current (initial settings: 120 kV, 185 μA), and slice thickness (0.5-2 mm). Across all tested scanning parameters, the massive and radio-opaque nature of the host rock did not allow for extraction of useful data.

Sampling for Scanning Electron Microscopy and Geochemical Analysis

The specimen was sampled extensively (total of 147 samples) across varying regions and tissues, largely concentrating on epidermal structures, but also including rock matrix, dermal bone (osteoderm), endochondral bone, gut contents, and fossil wood (Figure S3i). Samples we taken at three different intervals between Dec. 2016 and April 2017. The majority of the specimen was treated with adhesives (Paraloid B-72 and Paleobond penetrate stabilizer) during the preparation process, but several sections of the sacral region were collected as split blocks and were kept untreated. 103 samples were taken for electron microscopy from across the body, while 44 samples were taken for geochemical analyses. The geochemical samples largely concentrating on the untreated sacral region, but did also include samples from the main body of the animal. Samples for both analyses were taken with a scalpel by chipping/prying off small fragments. Those destined for SEM were carefully transferred over with a moistened tip onto an aluminum 12 mm SEM stub with double sided carbon tape, while geochemical samples were transferred on a clean scalpel blade onto sterilized aluminum foil. Samples were kept in plastic boxes for transport.

Scanning Electron Microscopy

Samples were coated with gold and analyzed in a Zeiss Sigma HD VP field emission SEM with an EDAX EBSD attached. Secondary Electron images were taken off the horn sheath and skin from a representative set of samples to search for melanosomes and to investigate the mode of preservation and the composition of the rock matrix (See also Figure S3ii and Supplemental Observations Under the Electron Microscope).

Time-of-Flight Secondary Ion Mass Spectroscopy

The samples for ToFSIMS analysis were mounted directly onto a sample holder using double-sided carbon tape or clean stainless steel screws and clips as appropriate.

Static SIMS analyses were carried out using an ION-TOF 'TOF-SIMS IV – 200' instrument (ION-TOF GmbH, Münster, Germany) of single-stage reflectron design [59]. Positive and negative ion spectra were obtained using a Bi_3^+ focused liquid metal ion gun at 25 keV energy, incident at 45° to the surface normal and operated in 'bunched' mode for high mass resolution. This mode used 20ns wide ion pulses at 10kHz repetition rate. Charge compensation was effected by low-energy (ca. 20 eV) electrons provided by a flood gun. The total ion dose density was 5×10^{16} ions m^{-2}. The topography of the sample surface and the ion gun mode of operation limited the mass resolution in this work to ca. $m/\Delta m = 2000$. The spatial resolution was limited by the primary ion beam diameter to ca. 4 μm.

Positive and negative ion static SIMS spectra were recorded from the outermost ca. 1nm of the sample surface at room temperature. Raw data containing the secondary ions recorded at each pixel was acquired with a 128 × 128 pixel raster and a field of view of 50 μm × 50 μm (see also Figure S3iii and Supplemental Results from the TOF SIMS).

Pyrolysis Gas Chromatography-Mass Spectrometry

Pyrolysis experiments were performed using a CDS Analytical 5250 pyroprobe equipped with an autosampler and coupled directly to an Agilent 6890 N gas chromatograph interfaced with a Waters Micromass Autospec-Ultima mass spectrometer. Approximately 300-700 μg of each sample was placed in a CDS quartz sample tube packed with a quartz wool plug followed by a quartz filler rod and a second plug of quartz wool. Internal standards comprising 50ng each of decafluorobiphenyl (DFB) and pyrene in pentane were then added to the samples immediately prior to analysis. Once loaded in the autosampler, the quartz tubes were dropped into the pyrolysis chamber where they were kept at 50°C for 5 s and then heated at 10°C/ms to 600°C and held for 20 s. The valve oven and transfer line were held at 300°C throughout the analysis. The thermal degradation products were transferred directly to a GC column held at 40°C. The GC was equipped with a DB-5MS column (60 m x 0.25 mm x 0.25 μm) and was operated in split mode with a 5:1 split and 1 mL/min He flow rate. The GC was held at 40°C for 2 min and then programmed to 310°C at 4°C/min where it was held for 20 min. The MS was operated in electron impact mode at 70 eV and scanned m/z 50–600 once per second. Analyses were conducted in duplicate with regularly interspersed blanks. Mass Lynx mass spectrometry software version 4.0 was used for data collection and processing. The identification of pyrolysis products was based on comparison of their mass spectra with library spectra (NIST MS Search 2.0) and by comparisons to data gathered previously [20] (see also Figure S3iv and Supplemental Results of Pyrolysis GC-MS).

Photography

Cross-Polarized Light Photography

In order to enhance color contrast for mapping the preservation and distribution of soft tissues across the specimen, a Lowell totalight equipped with a 750W tungsten bulb was set up with a polarizing gel filter in front [60]. The specimen was then wetted with water and photographed with a Nikon d800 dSLR camera and a 60mm f 2.8 Macro Nikkor lens with a polarizing filter mounted. Photos were then taken so that the polarizing filter is perpendicular to the orientation of the polarizing gel. This configuration ensures the filtering of any light that bounced off the surface of the specimen in resulting glare (see also Figures S4i and ii).

UV Fluorescence Photography

To identify any fluorescing minerals, such as calcium phosphate deposits, from the degraded keratin matrix the specimen was photographed illuminated with a short wave Superbright 2 (UV systems inc.) UV lamp using the same camera as for the cross-polarized light photography. Due to the faintness of the fluorescence, photos were taken with a long exposure - between 20-30 s (see also Figure S4iii).

QUANTIFICATION AND STATISTICAL ANALYSIS

Phylogenetic Methods

To determine the phylogenetic position of *Borealopelta markmitchelli*, it was scored into the morphological character/taxon matrix of Arbour et al. [14]. Although *B. markmitchelli* is known from a remarkably complete specimen, the majority of both cranial characters and postcranial endoskeletal characters are obscured by preserved integument. As a result, only 41/91 (45%) cranial and 4/62 (6%) postcranial could be coded along with 13/24 (54%) osteoderm characters, for a total of 58/177 (33%).

Several of the more incomplete and unstable, taxa included in the previous analysis [14] were removed: *Ahshislepelta minor*, *Alectopelta coombsi*, "Argentinian ankylosaur," *Hoplitosaurus marshi*, "Paw paw scuteling," *Struthiosaurus languedocensis*, *Struthiosaurus transylvanicus*, *Taohelong jinchengensis*, *Texasestes pleurohalio*, *Zarapelta sanjuanensis*, and *Zhejiangosaurus luoyangensis*. The resulting taxon character matrix consisted of 47 OTUs and 177 characters (Datafile S1 and S2). The character/taxon matrix was analyses in TNT (version 1.1) [61]. All characters we treated as unordered and equally weighted. The traditional search option with one random seed and 1000 replicates and tree bisection algorithm (TBR) was used to identify most parsimonious trees. A new technology search was also performed. Bootstrap analysis (1000 replicates) using TBR, and Bremer support values (from suboptimal trees) were also obtained to indicate clade support (see also Supplemental Phylogenetic Results and Figures 3 and S2).

DATA AND SOFTWARE AVAILABILITY

Specimen

The holotype of *Borealopelta* is deposited at the Royal Tyrrell Museum of Palaeontology, Drumheller, Alberta, under the accession number: TMP 2011.033.0001. Samples for SEM analyses and TOF SIMS are held at the TMP under the same accession number. Samples for py-GC-MS were consumed.

Nomenclature

This published work and the nomenclatural acts it contains have been registered in ZooBank, the online registration system for the International Commission on Zoological Nomenclature. ZooBank LSIDs (Life Science Identifiers) can be viewed by appending the LSID to the prefix http://zoobank.org/. The LSID for this publication is urn:lsid:zoobank.org:pub:39B2603A-CEF7-4657-B5D8-71CE295AA2E4. The electronic edition of this work was published in a journal with an ISSN and will be archived and made available from the following digital repository: CLOCKSS (http://www.clockss.org/clockss/Home).